METAMATERIALS

Three-dimensional mechanical metamaterials with a twist

Tobias Frenzel,[1] Muamer Kadic,[1,2,3] Martin Wegener[1,2]*

Rationally designed artificial materials enable mechanical properties that are inaccessible with ordinary materials. Pushing on an ordinary linearly elastic bar can cause it to be deformed in many ways. However, a twist, the counterpart of optical activity in the static case, is strictly zero. The unavailability of this degree of freedom hinders applications in terms of mode conversion and the realization of advanced mechanical designs using coordinate transformations. Here, we aim at realizing microstructured three-dimensional elastic chiral mechanical metamaterials that overcome this limitation. On overall millimeter-sized samples, we measure twists per axial strain exceeding 2°/%. Scaling up the number of unit cells for fixed sample dimensions, the twist is robust due to metamaterial stiffening, indicating a characteristic length scale and bringing the aforementioned applications into reach.

The concept of rationally designed human-made composite materials or metamaterials, together with advances in three-dimensional (3D) micro- and nanofabrication, has recently opened the door to mechanical properties that were previously inaccessible (*1*). By virtue of mechanical metamaterials, applications have come into reach that require ultralow mass densities (*2*–*4*), ultrastrong materials (*5*), deployable materials for space missions (*6*), protection by mechanical cloaking (*7*) or reusable mechanical shock-absorbing materials (*8*–*10*), programmable mechanical properties (*11*), reconfigurability (*12*), or nonreciprocal one-way isolation of forces (*13*). In addition to these quasistatic examples, mode conversion between longitudinal and transverse in-plane elastic waves has recently been achieved in 2D metamaterials (*14*). However, the elastic counterpart of optical activity in 3D chiral structures (*15*, *16*), converting one transverse linearly polarized elastic wave into the orthogonal transverse one, has been elusive.

In the static case, such "mechanical activity" is connected to the fact that an elastic solid cannot twist upon pushing or pulling on it within ordinary (Cauchy) continuum mechanics (Fig. 1), implying zero force-torque coupling. In essence, the solid cannot twist because the atomic unit cells in macroscopic bodies are so small that they can be seen as infinitesimally small volumes (*17*). Hence, there is no spatial scale. A pointlike object can be displaced, but there is no meaning in saying that it rotates or deforms.

Mathematically, Cauchy continuum mechanics is the generalization of Hooke's law in 1D, which states that the force is the product of the Hooke's spring constant and the displacement. In 3D, the stress tensor $\overleftrightarrow{\sigma}$ becomes the inner product of the elasticity tensor $\overleftrightarrow{C}$ and the strain tensor $\overleftrightarrow{\epsilon}$—i.e., $\sigma_{ij} = C_{ijkl}\,\epsilon_{kl}$, where we use the Einstein summation convention (*17*). $\overleftrightarrow{C}$ is invariant under space inversion, which converts left-handed structures into right-handed structures, whereas both $\overleftrightarrow{\sigma}$ and $\overleftrightarrow{\epsilon}$ change their sign (*17*). Therefore, Cauchy elasticity does not describe any chiral effects. The underlying approximation of treating a crystal unit cell as pointlike works if the unit cell is much smaller than the sample size and much smaller than the wavelength/λ of an elastic wave. In the static case, the wavelength is formally infinitely large, and only the ratio of sample size L to unit-cell size a matters. For Cauchy continuum mechanics, this means that the number of unit cells within a bar does not influence its properties because there is no spatial reference scale (mathematically, the scale is infinitesimally small). Cauchy continuum mechanics has been generalized toward linear micropolar continuum mechanics (*18*–*20*), which we will use below, and further toward higher-order gradients (*21*). Finally, outside of the linear regime, instabilities can lead to further unusual behavior (*22*). Here, however, we aim at the linear elastic regime.

We designed, fabricated, characterized, and mapped onto micropolar effective-medium parameters 3D chiral microstructured mechanical metamaterials with twist degrees of freedom going qualitatively beyond Cauchy elasticity and representing the counterpart of optical activity (*15*, *16*) in mechanics. We focus on the static case. The rational design makes our work distinct from previous experimental studies characterizing existing materials, such as bone (*23*, *24*) or granular composites (*25*), with respect to micropolar elasticity in the dynamic regime. There, any unusual observation also needs to be distinguished unambiguously from both viscoelasticity (*23*) and/or from the effects of a generally anisotropic dynamic mass-density tensor (*26*).

We designed the metamaterial unit cell (Fig. 1C) by extensive numerical optimization (figs. S1 to S4), bearing in mind fabrication restrictions in regard to the minimum accessible ratio of feature size to unit-cell size a. This makes our blueprint distinct from other recent ones (*27*). Our unit cell has four-fold rotational symmetry upon

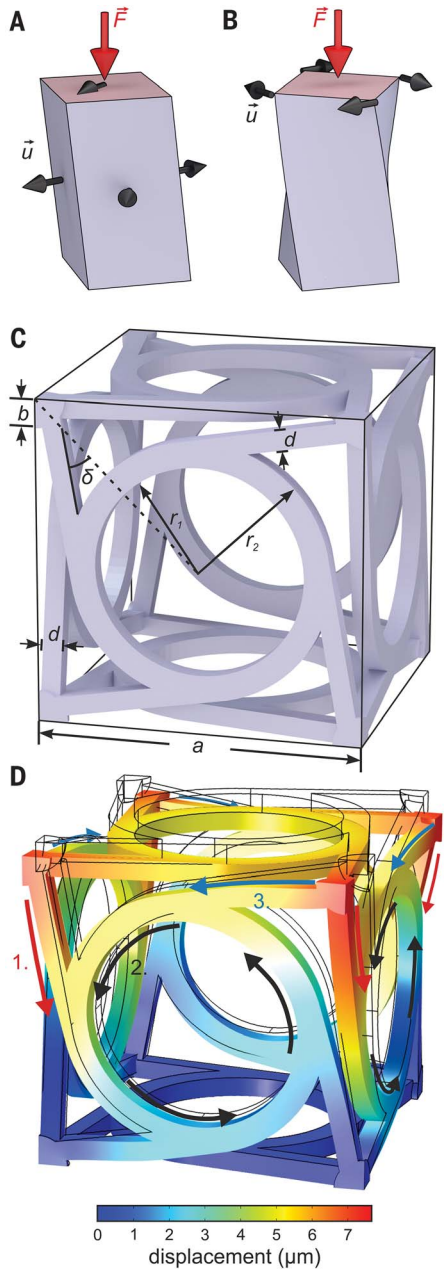

Fig. 1. Twist degrees of freedom in mechanics. (**A**) Pushing on an elastic material bar (red arrow) can make it expand or contract isotropically or anisotropically in the orthogonal directions. (**B**) A twist, however, is forbidden in ordinary linear (Cauchy) continuum mechanics. (**C**) Unit cell of a metamaterial crystal enabling the twist degree of freedom. The lattice constant a, the angle δ, the radii r_1 and r_2, and the widths b and d are indicated. (**D**) Calculated deformed cell and displacement under uniaxial loading. The arrows aid the discussion of the mechanism: 1. The arms connecting the corners with the rings move downward. 2. This motion leads to a rotation of the rings. 3. This rotation exerts forces onto the corners in the plane normal to the pushing axis, resulting in an overall twist of the unit cell around this axis (also see fig. S1).

[1]Institute of Applied Physics, Karlsruhe Institute of Technology, 76128 Karlsruhe, Germany. [2]Institute of Nanotechnology, Karlsruhe Institute of Technology, 76021 Karlsruhe, Germany. [3]Institut Franche-Comté Electronique, Mécanique, Thermique et Optique–Sciences et Technologies, UMR 6174, CNRS, Université de Bourgogne Franche-Comté, 25000 Besançon, France.
*Corresponding author. Email: martin.wegener@kit.edu

rotation around the three principal cubic axes. It is chiral—hence noncentrosymmetric—because it does not superimpose on its mirror image. Figure 1D illustrates the mechanism. We assembled an artificial metamaterial crystal by placing this unit cell onto a simple-cubic translational lattice with lattice constant a. We fabricated a large number of corresponding polymer microstructures by using 3D laser microprinting (Fig. 2) (*28*). For the static case, all twist effects must vanish in the limit of large sample extent L with respect to the unit-cell size a. Furthermore, within Cauchy continuum mechanics, the Hooke's spring constant of a bar with fixed extent is strictly independent of the number of unit cells within the bar. Thus, the crucial test is to investigate the effective mechanical properties upon changing the size of the unit cell, while fixing the shape and aspect ratios. After process optimization, we obtained a maximum scaling factor of $N = L/a = 5$ (Fig. 2).

To test our material experimentally, we fabricated a left-handed chiral metamaterial bar on top of an otherwise identical right-handed bar to keep the total torque at zero. This circumvents the problem of allowing for twist while pushing on a material bar (Fig. 1). Sliding boundary conditions can solve this issue in principle, but they are problematic on the microscale. Our setup allowed the middle of the sample to rotate while the top and bottom were fixed. We employed image cross-correlation analysis to track markers arranged onto a plate in the middle of the sample (Fig. 2C) to visualize the twist. We derived twist angles by tracking the displacement vectors of all markers and by analyzing these data in terms of a common rotation around the sample center axis (Fig. 2C and movie S1). Independently, we measured the axial displacement of the stamp pushing on the sample—hence the sample strain—and the axial force by a force cell. The derived azimuthal components of the displacement vectors (blue arrows) are comparable to the axial components (red arrows)—that is, the usually forbidden degrees of freedom have become as large as the ordinary ones.

A maximum twist angle exceeding 2°/% of axial strain is found for $N = 1$, with a total of $(N \times N \times 2N) \times 2 = 4$ unit cells (Fig. 3A). This value decreases by about 50% toward the maximum of $N = 5$, corresponding to a total of 500 unit cells. At the same time, the effective Young's modulus (i.e., Hooke's spring constant times the sample height, $4L$, divided by the sample cross section, L^2) increases by a factor of 10 when going from 4 to 500 unit cells. Within Cauchy continuum mechanics, the twist would be strictly zero and the stiffness constant. We repeated all experiments for achiral structures as controls—i.e., for $\delta = 0$ (compare with Fig. 1C) and with otherwise identical design parameters. As expected from Cauchy continuum mechanics and from symmetry, we found zero twist angles within the noise (blue data points in Fig. 3A) and constant effective Young's modulus (Fig. 3B) upon varying $N = 1,2,3,4,5$.

We compared our results for both chiral and achiral structures with numerical finite-element calculations for the same design parameters and fixed constituent material Young's modulus $E = 2.6$ GPa and Poisson's ratio $v = 0.4$ (*28*) (Fig. 3). We found agreement with our experiments in terms of the overall qualitative behavior. The remaining differences between experiment and theory are likely due to imperfections in sample fabrication in regard to the size scaling.

To interpret the observed twist in terms of effective material parameters, we needed to map the behavior onto a generalized effective-medium description. Such description must grasp the fact that the unit cell itself can rotate with respect to the lattice or be deformed. For negligible deformations in micropolar materials, a rotational vector field ϕ suffices, in addition to the usual displacement vector field $\boldsymbol{u}$, leading to the generalized linear elasticity equations (*18*–*20*)

$$\sigma_{ij} = C_{ijkl}\,\epsilon_{kl} + D_{ijkl}\,\varphi_{kl} \quad (1)$$

$$m_{ij} = A_{ijkl}\,\varphi_{kl} + B_{ijkl}\,\epsilon_{kl} \quad (2)$$

Here, $\overleftrightarrow{\sigma}$ is the usual stress tensor, $\overleftrightarrow{m}$ is the coupled stress tensor, $\epsilon_{kl} = \frac{\partial u_l}{\partial x_k} - \varepsilon_{klm}\,\phi_m$ and $\varphi_{kl} = \frac{\partial \phi_k}{\partial x_l}$ are the elements of the generalized strain tensors, and ε_{ijk} is the Levi-Civita symbol. $\overleftrightarrow{A}$, $\overleftrightarrow{B}$, $\overleftrightarrow{C}$, and $\overleftrightarrow{D}$ are the generalized rank-four elasticity tensors, with $B_{ijkl} = D_{klji}$. In general, these four tensors contain 196 independent material parameters. For the special case of cubic chiral materials relevant here, this number is reduced to 12 (*28*). For achiral micropolar media, the force-torque coupling terms vanish—i.e., $\overleftrightarrow{B} = \overleftrightarrow{D} = 0$, and the twist angle is zero. If additionally $\overleftrightarrow{A} = 0$ and $C_{ijkl} = C_{jikl} = C_{ijlk}$, ordinary Cauchy continuum mechanics is recovered.

Micropolar continuum mechanics also reproduced the overall measured behavior (Figs. 3 and

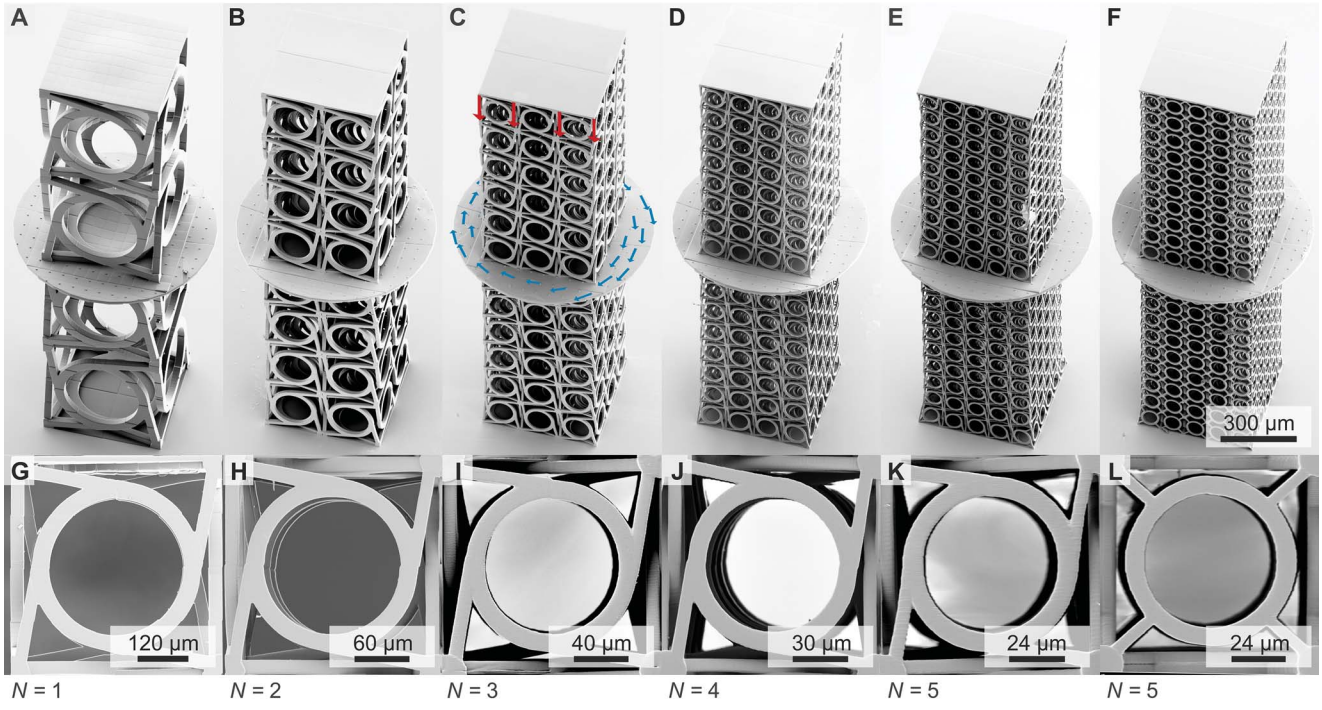

Fig. 2. Gallery of electron micrographs. (**A** to **E**) Polymer samples following the blueprint shown in Fig. 1C, fabricated using 3D laser microprinting. Arranging a left-handed metamaterial bar on top of a right-handed one enables twists without the need for sliding boundary conditions. (**G** to **K**) Changing the number of unit cells within the bars, while fixing all aspect ratios and outer dimensions, is crucial to investigate the breakdown of scalability associated with mechanical chirality. (**F**) and (**L**) are achiral controls. The measured azimuthal displacement vectors (blue) added in (C) indicate a twist upon pushing on the metamaterial bar. The axial displacement vectors are shown as red arrows (movie S1). All arrows are stretched by a factor of 5.

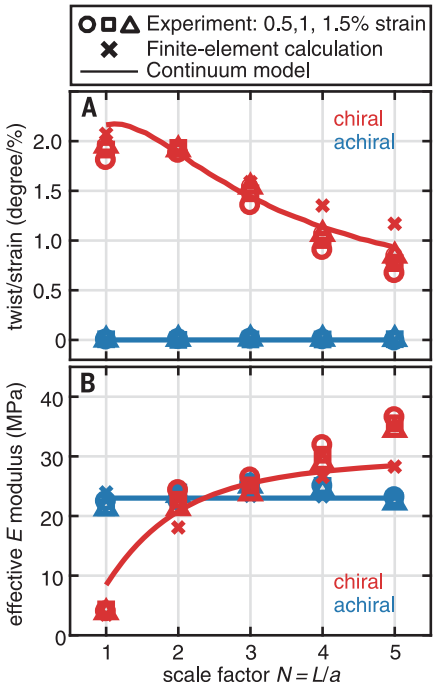

Fig. 3. Measured and calculated results. We vary the total number of unit cells ($N \times N \times 2N$) × 2 with $N = L/a$ = 1,2,3,4,5 while fixing the outer dimensions of the samples (compare Fig. 2). (**A**) Twist angle per axial strain versus N. (**B**) Effective Young's (E) modulus of the metamaterial bar versus N. Red (blue) symbols correspond to chiral (achiral) samples. Circles (0.5% strain), squares (1.0% strain), and triangles (1.5% strain) are measured. The statistical error bars are on the scale of the size of the symbols. The crosses are calculated in the linear regime. The solid red curves result from micropolar continuum mechanics (*28*) (Fig. 4B); the solid blue straight lines are the expectation from Cauchy continuum mechanics.

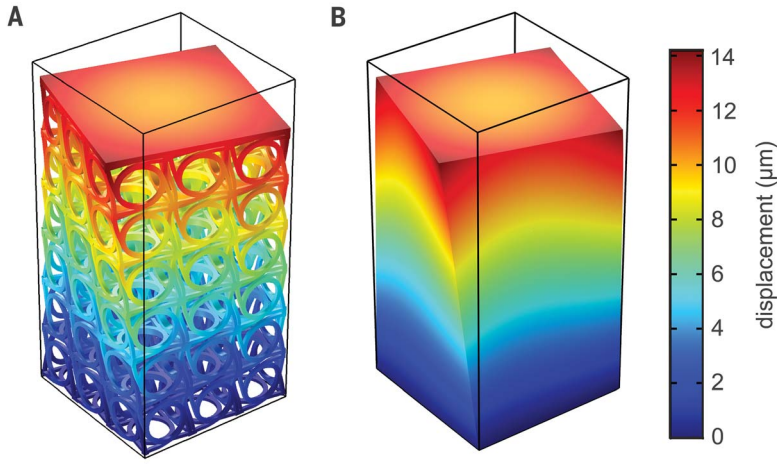

Fig. 4. Finite-element calculations. Structure and modulus of the displacement vector field on a false-color scale are overlaid. (**A**) Microstructure calculation for N = 3 (compare Fig. 2C). (**B**) Calculation following chiral micropolar continuum mechanics for $L = 3a$ with a = 500 μm (*28*). In both cases, the axial strain is 1%. The black lines indicate the sample boundaries for zero strain. For better visibility, the deformations have been multiplied by a factor of 10. The false-color scale shows the true displacements. All other parameters are as in Fig. 3 (*28*).

4B). Numerical calculations, extended to $L/a \gg 1$ (fig. S5), showed that the twist angle asymptotically decreases as $\propto (L/a)^{-1} = 1/N$. Upon axial loading, each unit-cell facet generates a transverse displacement, which adds up to a rotational deformation of the unit cell (fig. S1). Intuitively, the rotational displacement vectors of touching unit-cell facets in the bulk cancel each other, such that the overall material twist stems from open unit-cell facets at the metamaterial surface, leading to a scaling $\propto$ surface/volume $\propto 1/N$. The same competition between displacements of neighboring unit cells in the bulk also leads to an initial stiffening of the metamaterial with increasing N until the Young's modulus saturates when these competitions in the bulk become the dominating contribution.

Finally, dynamic band structure (fig. S6) and eigenmode calculations for the full microstructure (Fig. 1C) revealed a lifting of degeneracy for the two lowest-frequency transverse modes and corresponding circular eigen polarizations with opposite sense of rotation (fig. S7). In contrast to the static case with finite L/a and $\lambda/a \to \infty$, λ/a is finite and $L/a \to \infty$ for the band structures. Therefore effects beyond Cauchy continuum mechanics are allowed. As described in the introduction, Cauchy continuum mechanics is recovered in the limit that both $\lambda/a \to \infty$ and $L/a \to \infty$.

In conclusion, we have presented 3D chiral mechanical metamaterials showing twists per axial strain as large as 2°/%. The twist only decreases by a factor of two upon increasing the total number of unit cells from 4 to 500 for fixed sample dimensions due to a simultaneous increase of the metamaterial stiffness. This stiffening indicates a finite characteristic length scale. In sharp contrast, within Cauchy continuum mechanics, the twist would be strictly zero and the stiffness constant. We see our work as a step toward rationally designed artificial materials for which we can choose specific components of generalized elasticity tensors to obtain a wanted behavior, especially including degrees of freedom beyond Cauchy elasticity. Conversion of transverse modes by "mechanical activity" in analogy to optical activity in chiral optical materials is an example with immediate potential applications. Furthermore, it has been shown theoretically (*29*) that additional freedom in the elasticity tensors is needed in mechanics—for example, to steer force fields or mechanical waves around obstacles using static or dynamic cloaking structures, respectively, designed by coordinate transformations (*30*).

REFERENCES AND NOTES

1. M. Wegener, *Science* **342**, 939–940 (2013).
2. T. A. Schaedler *et al.*, *Science* **334**, 962–965 (2011).
3. X. Zheng *et al.*, *Science* **344**, 1373–1377 (2014).
4. L. R. Meza, S. Das, J. R. Greer, *Science* **345**, 1322–1326 (2014).
5. J. Bauer, A. Schroer, R. Schwaiger, O. Kraft, *Nat. Mater.* **15**, 438–443 (2016).
6. J. L. Silverberg *et al.*, *Science* **345**, 647–650 (2014).
7. T. Bückmann, M. Thiel, M. Kadic, R. Schittny, M. Wegener, *Nat. Commun.* **5**, 4130 (2014).
8. B. Florijn, C. Coulais, M. van Hecke, *Phys. Rev. Lett.* **113**, 175503 (2014).
9. T. Frenzel, C. Findeisen, M. Kadic, P. Gumbsch, M. Wegener, *Adv. Mater.* **28**, 5865–5870 (2016).
10. B. Haghpanah, L. Salari-Sharif, P. Pourrajab, J. Hopkins, L. Valdevit, *Adv. Mater.* **28**, 7915–7920 (2016).
11. C. Coulais, E. Teomy, K. de Reus, Y. Shokef, M. van Hecke, *Nature* **535**, 529–532 (2016).
12. J. T. B. Overvelde, J. C. Weaver, C. Hoberman, K. Bertoldi, *Nature* **541**, 347–352 (2017).
13. C. Coulais, D. Sounas, A. Alù, *Nature* **542**, 461–464 (2017).
14. J. M. Kweun, H. J. Lee, J. H. Oh, H. M. Seung, Y. Y. Kim, *Phys. Rev. Lett.* **118**, 205901 (2017).
15. J. B. Pendry, *Science* **306**, 1353–1355 (2004).
16. J. K. Gansel *et al.*, *Science* **325**, 1513–1515 (2009).
17. A. Sommerfeld, *Mechanics of Deformable Bodies: Lectures on Theoretical Physics*, Vol. 2 (Academic Press, New York, 1950).
18. R. S. Lakes, R. L. Benedict, *Int. J. Eng. Sci.* **20**, 1161–1167 (1982).
19. A. C. Eringen, *Microcontinuum Field Theories: I. Foundations and Solids* (Springer Science & Business Media, New York, 1999).
20. C. S. Ha, M. E. Plesha, R. S. Lakes, *Phys. Status Solidi, B Basic Res.* **253**, 1243–1251 (2016).
21. P. Seppecher, J.-J. Alibert, F. dell'Isola, *J. Phys. Conf. Ser.* **319**, 012018 (2011).
22. S. Babaee *et al.*, *Adv. Mater.* **25**, 5044–5049 (2013).
23. R. S. Lakes, *J. Biomech. Eng.* **104**, 6–11 (1982).
24. J. F. C. Yang, R. S. Lakes, *J. Biomech. Eng.* **103**, 275–279 (1981).
25. A. Merkel, V. Tournat, V. Gusev, *Phys. Rev. Lett.* **107**, 225502 (2011).
26. G. W. Milton, J. R. Willis, *Proc. R. Soc. Lond. Ser. A* **463**, 855–880 (2007).
27. M.-H. Fu, B.-B. Zheng, W.-H. Li, *Compos. Struct.* **176**, 442–448 (2017).
28. Materials and methods are available as supplementary materials.
29. G. W. Milton, M. Briane, J. R. Willis, *New J. Phys.* **8**, 248 (2006).
30. A. Diatta, S. Guenneau, *Appl. Phys. Lett.* **105**, 021901 (2014).

ACKNOWLEDGMENTS

We acknowledge support by the Helmholtz program Science and Technology of Nanosystems, including the Virtual Materials project,the Hector Fellow Academy, the Karlsruhe School of Optics and Photonics, and the Karlsruhe Institute of Technology Nanostructure Service Laboratory. M.K. acknowledges support by the Labex ACTION program (contract ANR-11-LABX-0001-01) and the French "Investissements d'Avenir" program, project ISITE-BFC (contract ANR-15-IDEX-03). Data are available in the main text and the supplementary materials.

SUPPLEMENTARY MATERIALS

www.sciencemag.org/content/358/6366/1072/suppl/DC1
Materials and Methods
Supplementary Text
Figs. S1 to S7
Movie S1
References

24 July 2017; accepted 18 October 2017
10.1126/science.aao4640

Science

Three-dimensional mechanical metamaterials with a twist

Tobias Frenzel, Muamer Kadic and Martin Wegener

Science **358** (6366), 1072-1074.
DOI: 10.1126/science.aao4640

Getting twisted with metamaterials

In the classical picture of solid mechanics, deformation in response to stress is constrained owing to limitations on the degrees of freedom. For instance, when you push on a material, you do not expect it to twist in response. Frenzel *et al.* designed a mechanical metamaterial with a pronounced twist to the left or right when pushed (see the Perspective by Coulais). Designing this type of chirality for a macroscopic material is unexpected, but it points to a more general strategy for developing materials with unusual deformation behavior.

Science, this issue p. 1072; see also p. 994